Journal of Innovative Optical Health Sciences
Vol. 2, No. 1 (2009) 27–35

World Scientific
www.worldscientific.com

ULTRASHORT PULSE MULTISPECTRAL NON-LINEAR OPTICAL MICROSCOPY

ADAM M. LARSON*, ANTHONY LEE*, PO-FENG LEE*,
KAYLA J. BAYLESS† and ALVIN T. YEH*,‡

*Department of Biomedical Engineering
Texas A&M University
College Station, Texas, USA

†Department of Molecular and Cellular Medicine
Texas A&M Health Science Center
College Station, Texas, USA
‡ayeh@tamu.edu

Ultrashort pulse, multispectral non-linear optical microscopy (NLOM) is developed and used to image, simultaneously, a mixed population of cells expressing different fluorescent protein mutants in a 3D tissue model of angiogenesis. Broadband, sub-10-fs pulses are used to excite multiple fluorescent proteins and generate second harmonic in collagen. A 16-channel multispectral detector is used to delineate the multiple non-linear optical signals, pixel by pixel, in NLOM. The ability to image multiple fluorescent protein mutants and collagen, enables serial measurements of cell-cell and cell-matrix interactions in our 3D tissue model and characterization of fundamental processes in angiogenic morphogenesis.

Keywords: Two-photon excited fluorescence; second harmonic generation; multiple molecular imaging; angiogenesis.

1. Introduction

Optical molecular imaging is an emerging field comprising several techniques that provide information at the molecular, cellular, tissue, and whole-organism length scales.[1] The emergence of these optical techniques has coincided with the development of post-genomic technologies that enable the characterization of living systems with unprecedented precision. Modern experimental biology can characterize the molecular profile or "state" of a cell or tissue with destructive readouts and assays capable of monitoring tens of thousands of molecules simultaneously. Quantitative readouts and high-throughput assays have highlighted the complexity of living systems and reinforced the appreciation of multiple biomolecular contributions to fundamental biological phenomena.

Optical techniques have a complementary ability to modern experimental biology of performing measurements on individual specimens over a time course, non-destructively, thereby providing unique insight into biological processes that are inherently dynamic. Non-linear optical microscopy (NLOM), in particular, is touted for its ability to render high resolution images from deep within intact living tissues. The minimally invasive nature of NLOM and its ability to provide morphological and chemo-physiological information concurrently within tissues makes it well suited to follow response and progression resulting from pathologically, chemically, or mechanically induced stressors. Additionally, the wide range of detectable contrast mechanisms available to NLOM can be used to characterize the molecular biology within a microscopic milieu.

Second harmonic generation (SHG) and two-photon excited fluorescence (TPF) are two non-linear optical signals used for image rendering in NLOM. Generation of second harmonic imposes symmetry and long-range molecular order requirements, making it a constituent-specific, intrinsic-contrast mechanism localized to collagen,[2–4] cardiac myocytes[5] and muscle sarcomeres.[6] The TPF of NAD(P)H,[7–13] flavins,[14] and mature elastin[15] provides morphological, spectroscopic, and metabolic information surrounding cellular processes. However, endogenous fluorescence spectra tend to be broad, featureless, and overlapping which complicate their spectral segmentation by constituent. Morphological and functional imaging by NLOM can be expanded further with the use of exogenous markers specific to tissue constituents.[16] This includes transgenic strategies to genetically encode fluorescent proteins as reporters of particular biomolecules. Fluorescent proteins are increasingly being used to observe developmental events as they can be widely expressed in the cytoplasm or inserted into genes for specific cytogenetic profiling. These techniques are well matched to emerging genomic and proteomic technologies[17,18] enabling the development of fluorescent (protein) optical probes[19] and nanotechnologies allowing multifunctional imaging in real-time with minimal or no invasion.[20,21]

Herein, we report the development of an optical fiber coupled, multispectral detector for NLOM that measures, pixel by pixel, non-linear optical signal intensity in 16 discrete channels simultaneously. Multispectral NLOM is used to image a mixed population of primary human endothelial cells expressing cyan (CFP), green (GFP), and yellow fluorescent proteins (YFP) in an *in vitro* model that mimics angiogenesis.[22,23] Endothelial cells are stimulated to penetrate a 3D collagen matrix and assemble into multicellular structures surrounding an open lumen. Broadband, sub-10-fs pulses are used to excite the three fluorescent protein mutants and SHG in collagen matrix simultaneously. Sub-10-fs pulses require careful control of the pulse duration at the sample,[24] which allows the contribution of all spectral components to fluorophore excitation. Furthermore, simultaneous excitation of multiple contrast agents greatly reduces the photo and thermal damage associated with rescanning the sample.[25] We show that ultrashort pulse, multispectral NLOM may be used to excite and delineate multiple constituents in a living biological system.

2. Materials and Methods

2.1. *Ultrashort pulse multispectral NLOM*

The ultrashort pulse NLOM system used in this study has been previously described by our group.[24] Briefly, broadband, sub-10-fs pulses generated by a Ti:Al_2O_3 (75 MHz repetition rate) oscillator pumped by a frequency doubled Nd:YVO_4 solid-state laser are coupled into an upright microscope. Interferometric autocorrelation measurement of ultrashort pulses at the focus is used to adjust the number of reflections from dispersion compensation mirrors and minimize phase distortions. Pulse duration at the sample plane is measured to be 12.7 fs using a Zeiss 40X Achroplan (0.8 NA) objective. The laser pulse spectrum encompasses nearly the entire gain of Ti:Al_2O_3 and is shown in Fig. 1(a) with center wavelength of 800 nm and bandwidth (FWHM) of 125 nm. From the pulse spectrum, its two-photon excitation power spectrum can be calculated using second-order perturbation theory as,[17,26,27]

$$T(\omega) = \left| \int_0^\infty E(\omega/2 + \Omega)) E(\omega/2 - \Omega) d\Omega \right|^2, \quad (1)$$

where $|E(\omega)|^2$ is the pulse spectrum and Ω is an iterative variable that ensures integration over all possible frequency combinations such that $\omega = \omega_i + \omega_j$. The two-photon excitation spectrum, $T(\omega)$, shown in Fig. 1(b) was calculated using Eq. (1), the pulse spectrum of Fig. 1(a) and assuming transform limited pulses at the focus. For a given pulse shape, the integral of $T(\omega)$ is inversely proportional with pulse duration, i.e., the area under the spectrum shown in Fig. 1(b) is larger than that for 100 fs pulses by a factor of $\sim$ 10. (Direct comparisons may be found in Ref. 17). For TPF, the probability of non-resonant two-photon absorption is proportional to the overlap integral,[28,29]

$$\Gamma \propto \int_{-\infty}^{\infty} \gamma(\omega) T(\omega) d\omega, \quad (2)$$

where $\gamma(\omega)$ is the molecular two-photon absorption spectrum. When the molecular absorption is frequency invariant across the pulse excitation spectrum, i.e., $\gamma(\omega) \rightarrow \gamma$, it follows that TPF intensity varies inversely with pulse duration. However, for broadband pulses of ultrashort duration, this invariance condition no longer holds, but the

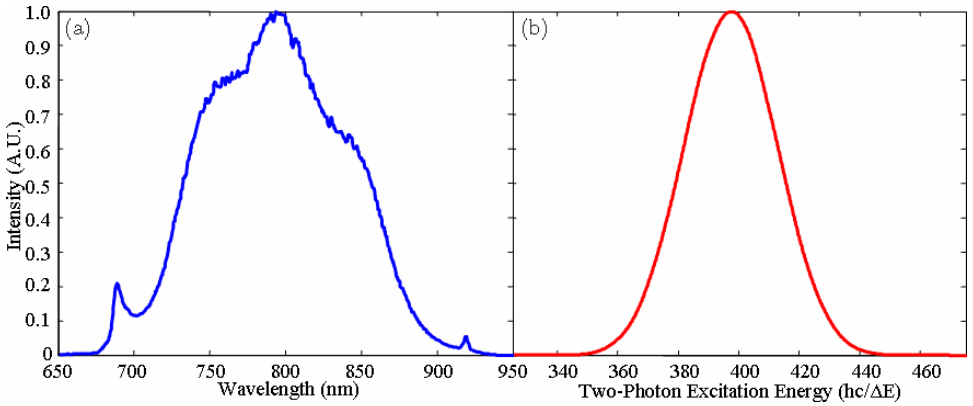

Fig. 1. Sub-10-fs laser spectrum (a) and calculated two-photon excitation power spectrum (b).

broad excitation profile of $T(\omega)$ may be used to enhance overlap with multiple molecular absorption spectra.[30]

The non-linear optical microscopy spectral imaging system (NOMSIS) software was developed using National Instruments LabVIEW and raw data processed using MATLAB. Multispectral imaging was carried out using a home-built fiber-coupled Czerny-Turner spectrometer in a Littrow configuration containing a 16-channel multianode PMT (R5900U-00-L16, Hamamatsu). A large core (910 μm) multimode optical fiber is used to transfer the collected signal from the microscope to the remotely located spectrometer. The optical fiber is placed in a conjugate plane to the back focal aperture (BFA) of the objective lens. This creates a pivot point on the fiber aperture analogous to the pivot point of the scan mirrors on the BFA. Therefore, as the beam is scanned, the point on the fiber aperture is stationary. Configured in this manner, the core diameter of the fiber does not determine the field-of-view for the resulting image, rather, it determines the overall signal intensity. Field-of-view is ultimately limited by the numerical aperture, NA (= 0.22) of the collection fiber. This layout is shown schematically in Fig. 2(a).

Divergent light from the fiber aperture (entrance slit) is collimated using an achromatic lens corrected for the visible range (d = 38.1 mm, f = 90.0 mm). To appropriately demagnify the entrance slit, an f = 75.0 mm lens was used to focus the diffracted beam onto the detector. A diffraction grating with 700 grooves/mm blazed at 530 nm (53-067-455R, Richardson Grating) yields a spectral range of 280 nm. The center wavelength of the spectrometer is set to 490 nm giving a spectral range of 350–630 nm. The linear dispersion and spectral resolution are 17.6 nm/mm and 14.2 nm (given by the pass band of the exit slit), respectively. The multianode PMT acts as a series of individual exit slits with a single element detector behind each slit. The low resolution and spacing between detector elements limits the impact of spectrometer aberrations on resolution. Detector calibration was done by tilting the diffraction grating to obtain the correct emission spectra of two reference (FITC and TRITC) fluorescent dyes. The optical path of the spectrometer is shown schematically in Fig. 2(b).

The output from each channel is sent to a bank of 16 independent preamplifier/discriminators (F-100T, Advanced Research Instruments). The discriminators convert the current outputs from the PMTs into TTL pulses when specified thresholds have been exceeded; thresholds are independently determined for each channel. For maximum sensitivity, the thresholds were set at the lowest level while still discriminating against background (and electronic) noise. The TTL pulses are input to two, 8-channel counting cards (PCI-6602, National Instruments) and used for image construction within NOMSIS.

The NOMSIS outputs sawtooth waveforms to driver boards for dual-axis galvanometer mirrors through a data acquisition card (PCI-6259, National Instruments) which control field-of-view and scanning speed. Pixel dwell time and field-of-view can be set with proper frequency and amplitude values, respectively. Frame rates have been programmed to be as fast as 1 Hz or as slow as 0.0625 Hz for maximum signal-to-noise. In order to synchronize the mirrors to the counter cards, a frequency-dependent internal timer acts as a trigger for all the three cards. This trigger activates

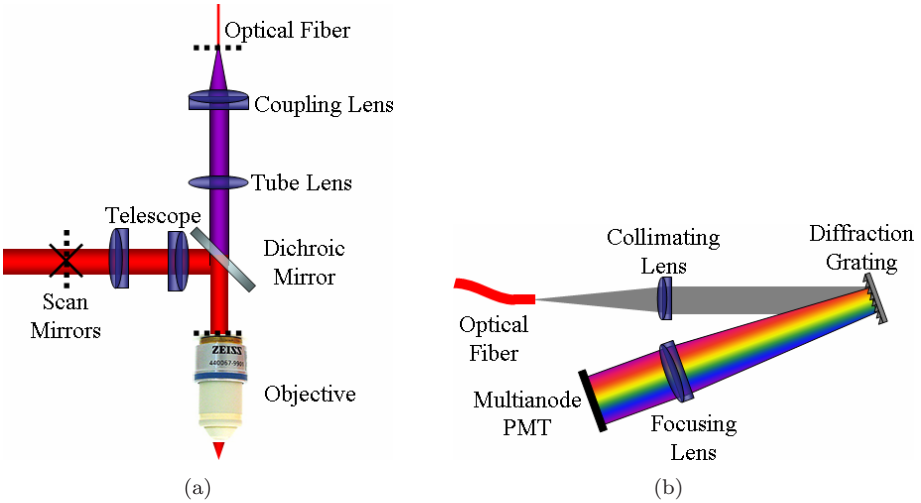

Fig. 2. (a) Schematic of the optics necessary to focus collected signal from the objective into the optical fiber. (b) Schematic of the Czerny-Turner spectral detector. Light from the fiber is collimated, diffracted off the grating, and focused onto the multianode PMT array.

the signal generation and data collection simultaneously on the first rising edge of the timer.

Once collected, the pulse counts are stored as a $256 \times 256 \times 16$ 3-dimensional integer array. The spectral data stacks are saved in binary format for post-processing analysis in MATLAB. If desired, the software can be fully automated to translate the stage and acquire 5-dimensional stacks (X, Y, Z, λ, t) without human intervention.

2.2. *Cell and tissue culture*

Primary human umbilical vein endothelial cells were propagated as described.[23] Stable endothelial cell lines expressing fluorescent proteins were generated using a recombinant lentivirus system (Invitrogen). The enhanced green fluorescent protein (EGFP) pLenti6/V5 expression vector was a kind gift of George Davis (Columbia, MO). Cyan fluorescent protein (CFP) and yellow fluorescent protein (YFP) were amplified from pAmCyan1-C1 and pZsYellow1-C1 vectors (BD Biosciences), respectively. Inserts were inserted into the pLenti6/V5 TOPO vector using standard methods. Following sequence analysis, lentiviruses were prepared as previously described.[31] Cells underwent blasticidin selection (5 μg/mL) for two weeks before being frozen down at passage 3 or used in experiments.

Collagen matrices (3.6 mg/mL, BD Biosciences) were assembled as previously described[32] before incorporating 1 μM S1P. After thorough mixing, 1 mL of collagen mixture was added per well of a Falcon 12-well plate (Becton Dickinson). Matrices were allowed to polymerize and equilibrate for 20 minutes at 37°C in CO_2 incubator prior to seeding 3.6×10^5 cells per well in serum-free Medium 199 (Invitrogen) containing reduced serum supplement II (RSII), recombinant VEGF (40 ng/mL, Upstate Biotechnologies), recombinant basic FGF (40 ng/mL, Upstate Biotechnologies), ascorbic acid (50 μg/mL) and Phorbol 12-myristate 13-acetate (TPA, 50 ng/mL, Sigma Aldrich). After allowing endothelial cells to attach to the collagen matrix surface for 20 minutes, the seeded gels were covered with 3 mL of identical serum-free media. Cultures were allowed to grow for 48 hours and imaged at 12-hour intervals between 48 and 72 hours. For imaging, the medium was removed and replaced with phosphate-buffered saline. After images were acquired, the medium was replaced and cultures were returned to the incubator.

3. Results

In our 3D model, endothelial cells are induced to invade the underlying collagen matrix and form angiogenic structures with patent lumens. The TPF from fluorescent proteins are spectrally distinct from SHG in collagen and therefore can be spectrally segmented. Spectral segmentation of TPF is shown in Fig. 3(a) where GFP expressing endothelial cells following 18 hours in culture are observed by NLOM to sprout from the confluent monolayer and form invading structures. The TPF and SHG images may be overlaid and false color applied to show morphologies of angiogenic patterning

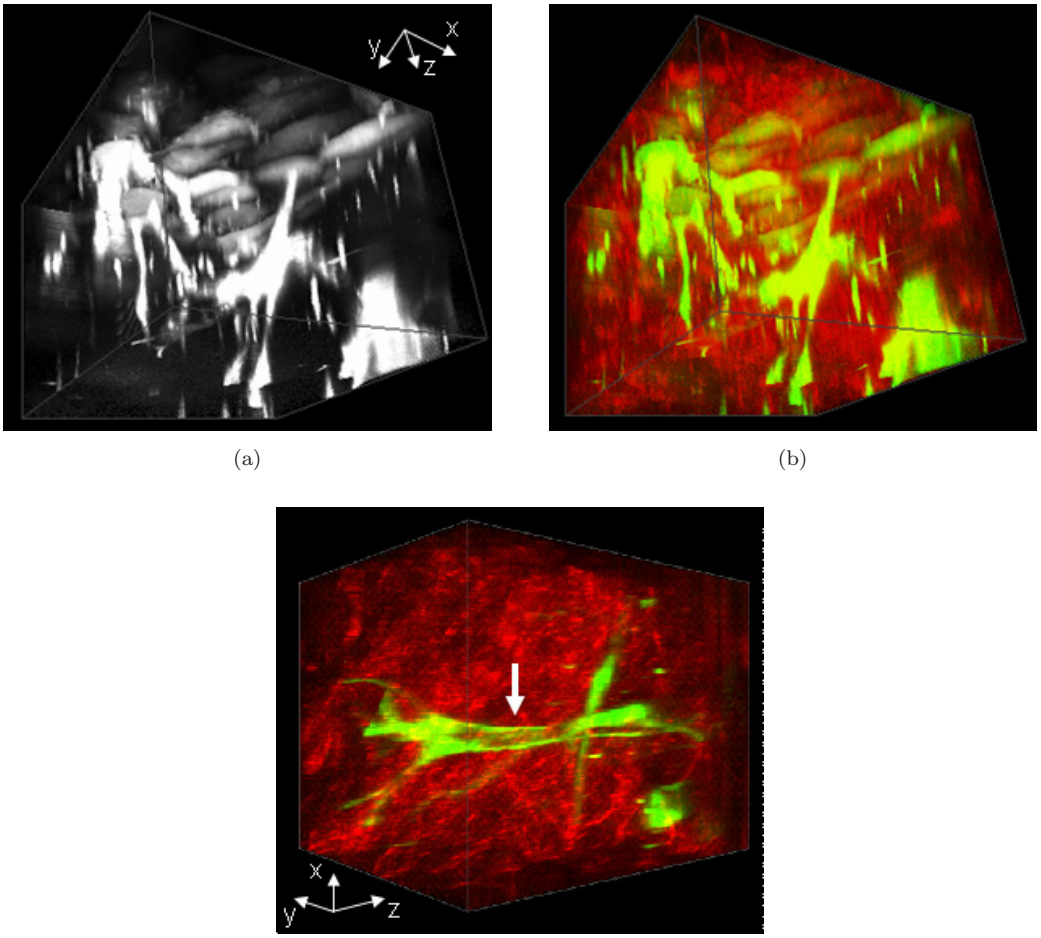

(a) (b)

(c)

Fig. 3. (a) Grayscale image showing the TPF from GFP expressing endothelial cells ($168 \times 168 \times 180\,\mu$m). (b) Three-dimensional reconstruction of sprout invasion (green) from the monolayer into the extracellular matrix (red). (c) Lumen formation after endothelial sprout invasion (green, white arrow) into extracellular matrix (red) ($150 \times 160 \times 225\,\mu$m).

(green) within the collagen matrix (red) as shown in Fig. 3(b). Following 36 hours in culture, lumens form within angiogenic structures. A representative 3D rendering is shown in Fig. 3(c) where a lumen is indicated by the absence of both TPF and SHG.

The NLOM has been used to characterize this *in vitro* 3D model of angiogenesis consisting of GFP expressing endothelial cells invading into collagen matrices. Endothelial cells have been observed to alter collagen matrices while undergoing invasion, migration, and lumen formation.[23] While this model provides spectrally distinct signals to characterize cells, matrix, and their points of interactions, cell-cell interactions are less obvious within a homogeneous endothelial cell population (Fig. 3).

To identify individually labeled endothelial cells, primary cell lines stably expressing CFP, GFP, and YFP were generated using recombinant lentiviruses (Section 2). The TPF from all three fluorescent proteins could be excited using our broadband, ultrashort pulse laser. The TPF spectra for the individual fluorescent proteins were obtained "*in vivo*" by imaging confluent homogeneous endothelial cells populations seeded directly onto the bottom of a 12-well plate. The TPF spectra are shown in Fig. 4 normalized to peak intensity.

To identify individually labeled endothelial cells within invading structures, a mixed population of CFP-, GFP-, and YFP- expressing endothelial cells was seeded on the surface of a collagen matrix and allowed to invade and penetrate collagen matrices. A representative NLOM image is shown in Fig. 5 from one such structure near the endothelial cell monolayer following 60 hours in culture. Numbered spectra are shown corresponding with regions demarked in the NLOM image. False color has been applied to the NLOM image according to spectral profile from each pixel. The NLOM imaging

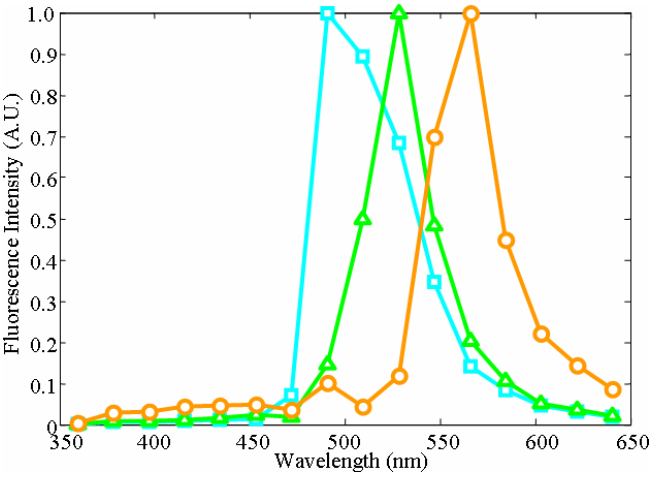

Fig. 4. TPF spectra of CFP (cyan, square), GFP (green, triangle) and YFP (orange, circle) fluorescent proteins. Individual spectra were obtained from a confluent monolayer of endothelial cells expressing fluorescent protein.

using SHG in collagen is shown in grayscale. A representative spectrum of predominantly SHG is shown from Region 1 containing collagen with a prominent peak at 400 nm. The SHG spectrum is discretized by the limited number of detection channels, but compares reasonably with the calculated second harmonic spectrum in terms of peak wavelength and spectral width (cf. Fig. 1(b)). There is also a broad signal corresponding to two-photon fluorescence from collagen.[12]

Green false color was applied to cells expressing GFP. Emission spectrum is shown from a region (2) containing a GFP- expressing endothelial cell and has a profile characteristic of GFP TPF (cf. Fig. 4). Yellow and cyan colors were applied to endothelial cells expressing YFP and CFP, respectively (see Regions 3 and 4). Regional emission spectra exhibit characteristic TPF profile of YFP and CFP when compared with spectra shown in Fig. 4. Regional spectrum from lumen (Region 5), which is devoid of both SHG and TPF, indicates baseline signal levels in counts per pixel.

4. Discussion

NLOM imaging has attributes conducive for serial measurements that can characterize biological response and/or progression of phenomena over a time course in individual specimens. Localized excitation of NLOM eliminates out-of-plane photobleaching of fluorophores that can plague linear optical techniques such as laser scanning confocal microscopy. In addition, non-absorptive processes such as SHG may be utilized that are not subject to in-plane photobleaching. For multiple molecular studies by NLOM utilizing narrowband, pulses $\geqslant 100$ fs, these advantages may be mitigated by the need for multiple scans wherein the laser central wavelength is tuned to (local) maximum TPF

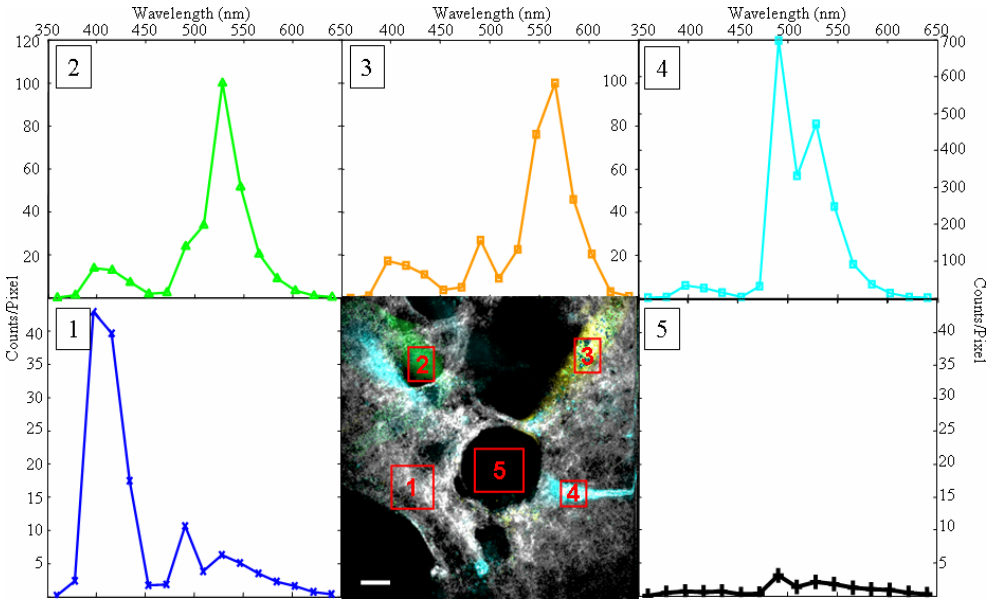

Fig. 5. Multiple molecular imaging of angiogenic endothelial cells within collagen matrix. Region 1: Spectra of SHG and TPF from collagen; Region 2: Endothelial cell expressing GFP; Region 3: YFP; Region 4: CFP; and Region 5: Spectrum from lumen. Scale bar 15 μm.

excitation of each fluorophore. Alternatively, the narrowband laser could be tuned to some optimum wavelength for all fluorophores thereby accepting some compromise in TPF excitation.

In this study, we demonstrate simultaneous excitation and detection of multiple fluorescent proteins as well as SHG in collagen. The merits of simultaneous multifluorophore excitation with ultrashort laser pulses enable chronological or time-lapse studies with higher non-linear optical signal generation than when using longer duration pulses.[30] The experimental configuration of coupling broadband, ultrashort pulses with multispectral detection for NLOM may prove useful in delineating the dynamics of multiple biomolecules and their concerted/competing contributions toward a biological effect. The implementation of multispectral detection has been demonstrated previously using tunable filters,[33] multianode PMT arrays[34] (with photon counting as in this study),[35] and charge-coupled device cameras,[36] albeit coupled with narrowband excitation sources. In these experimental configurations, judicial narrowband excitation may be used in conjunction with multispectral detection to help delineate multiple contributors to an emission spectrum. Indeed, controlling phase of ultrashort laser pulses can result in selective excitation of fluorophores.[25,28,29,37] More recently, synchronous laser scanning with central wavelength tuning was demonstrated for hyperspectral imaging of endogenous constituents in tissues.[38]

We created a mixed population of endothelial cells expressing different fluorescent protein mutants to characterize cell-cell interactions and arrangement within angiogenic sprouts. Our initial study mixed three endothelial cell populations expressing CFP, GFP, and YFP. Our data suggest that additional populations expressing fluorescent proteins with emission maxima to longer and shorter wavelengths could be incorporated into our 3D angiogenesis model and delineated with our multispectral detector, assuming ample excitation by the ultrashort laser pulse. This strategy is amenable to incorporation of time-lapse analyses to track and quantify the interactions of individual cells within tube-like structures and the surrounding 3D collagen matrix. An alternative strategy to delineate cell-cell interactions has been demonstrated in murine neurons where each expresses different amounts of three fluorescent proteins. Termed "Brainbow", each fluorescent protein acts as a primary color in the image, creating 10 hues.[39] We submit these trangenesis strategies with NLOM and these can be extended to illuminate fundamental molecular biology of dynamic biological processes by creating reporters for coding and non-coding sequences.

Acknowledgments

We thank Dr George Davis (University of Missouri, Columbia) for the pLenti6/V5 vector expressing EGFP. This work was funded by American Heart Association SDG (#0530020N) to KJB, National Institutes of Health (EB008366) and NSF Early Career Faculty Development Award (CAREER) to ATY. Equipment lists, schematics, and software of the NLOM system are available upon request. Please visit http://biomed.tamu.edu/tml.

References

1. Du, W., Wang, Y., Luo, Q. and Liu, B. F., "Optical molecular imaging for systems biology: from molecule to organism," *Anal. Bioanal. Chem.* **386**, 444–457 (2006).
2. Stoller, P., Reiser, K. M., Celliers, P. M. and Rubenchik, A. M., "Polarization-modulated second harmonic generation in collagen," *Biophys. J.* **82**, 3330–3342 (2002).
3. Williams, R. M., Zipfel, W. R. and Webb, W. W., "Interpreting second-harmonic generation images of collagen I fibrils," *Biophys. J.* **88**, 1377–1386 (2005).
4. Campagnola, P. J., Wei, M.-d., Lewis, A. and Loew, L. M., "High-resolution non-linear optical imaging of live cells by second harmonic generation," *Biophys. J.* **77**, 3341–3349 (1999).
5. Boulesteix, T., Beaurepaire, E., Sauviat, M. P. and Schanne-Klein, M. C., "Second-harmonic microscopy of unstained living cardiac myocytes: measurements of sarcomere length with 20-nm accuracy," *Opt. Lett.* **29**, 2031–2033 (2004).
6. Plotnikov, S. V., Millard, A. C., Campagnola, P. J. and Mohler, W. A., "Characterization of the myosin-based source for second-harmonic generation from muscle sarcomeres," *Biophys. J.* **90**, 693–703 (2006).
7. Piston, D. W., Masters, B. R. and Webb, W. W., "Three-dimensionally resolved NAD(P)H cellular metabolic redox imaging of the *in situ* cornea with two-photon excitation laser scanning microscopy," *J. Microsc.* **178**, 20–27 (1995).
8. Masters, B. R., So, P. T. and Gratton, E., "Multiphoton excitation fluorescence microscopy and spectroscopy of *in vivo* human skin," *Biophys. J.* **72**, 2405–2412 (1997).

9. Huang, S., Heikal, A. A. and Webb, W. W., "Two-photon fluorescence spectroscopy and microscopy of NAD(P)H and flavoprotein," *Biophys. J.* **82**, 2811–2825 (2002).
10. Rocheleau, J. V., Head, W. S. and Piston, D. W., "Quantitative NAD(P)H/flavoprotein autofluorescence imaging reveals metabolic mechanisms of pancreatic islet pyruvate response," *J. Biol. Chem.* **279**, 31780–31787 (2004).
11. Wu, Y. and Qu, J. Y., "Two-photon autofluorescence spectroscopy and second-harmonic generation of epithelial tissue," *Opt. Lett.* **30**, 3045–3047 (2005).
12. Zoumi, A., Yeh, A. and Tromberg, B. J., "Imaging cells and extracellular matrix *in vivo* by using second-harmonic generation and two-photon excited fluorescence," *Proc. Natl. Acad. Sci.* USA **99**, 11014–11019 (2002).
13. Yeh, A. T., Nassif, N., Zoumi, A. and Tromberg, B. J., "Selective corneal imaging using combined second-harmonic generation and two-photon excited fluorescence," *Opt. Lett.* **27**, 2082–2084 (2002).
14. Konig, K., "Multiphoton microscopy in life sciences," *J. Microsc.* **200**, 83–104 (2000).
15. Konig, K., Schenke-Layland, K., Riemann, I. and Stock, U. A., "Multiphoton autofluorescence imaging of intratissue elastic fibers," *Biomaterials* **26**, 495–500 (2005).
16. Friedl, P., "Dynamic imaging of cellular interactions with extracellular matrix," *Histochem. Cell Biol.* **122**, 183–190 (2004).
17. Yeh, A. T., Gibbs, H., Hu, J.-J. and Larson, A. M., "Advances in non-linear optical microscopy for visualizing dynamic tissue properties in culture," *Tissue Eng. B Rev.* **14**, 119–131 (2008).
18. Fuller, C. E., Wang, H., Zhang, W., Fuller, G. N. and Perry, A., "High-throughput molecular profiling of high-grade astrocytomas: the utility of fluorescence *in situ* hybridization on tissue microarrays (TMA-FISH)," *J. Neuropathol. Exp. Neurol.* **61**, 1078–1084 (2002).
19. Gross, S. and Piwnica-Worms, D., "Spying on cancer: molecular imaging *in vivo* with genetically encoded reporters," *Cancer Cell* **7**, 5–15 (2005).
20. Kumar, S. and Richards-Kortum, R., "Optical molecular imaging agents for cancer diagnostics and therapeutics," *Nanomed.* **1**, 23–30 (2006).
21. Gao, X. and Nie, S., "Molecular profiling of single cells and tissue specimens with quantum dots," *Trends. Biotechnol.* **21**, 371–373 (2003).
22. Bayless, K. J. and Davis, G. E., "Sphingosine-1-phosphate markedly induces matrix metalloproteinase and integrin-dependent human endothelial cell invasion and lumen formation in three-dimensional collagen and fibrin matrices," *Biochem. Biophys. Res. Commun.* **312**, 903–913 (2003).
23. Lee, P.-F., Yeh, A. T. and Bayless, K. J., "Nonlinear optical microscopy reveals invading endothelial cells anisotropically alter three-dimensional collagen matrices," *Exp. Cell Res.* (forthcoming) (2008).
24. Larson, A. M. and Yeh, A. T., "*Ex vivo* characterization of sub-10-fs pulses," *Opt. Lett.* **31**, 1681–1683 (2006).
25. Xi, P. Andegeko, Y., Weisel, L. R., Lozovoy, V. V. and Dantus, M., "Greater signal, increased depth, and less photobleaching in two-photon microscopy with 10 fs pulses," *Opt. Commun.* **281**, 1841–1849 (2008).
26. Meshulach, D. and Silberberg, Y., "Coherent quantum control of two-photon transitions by a femtosecond laser pulse," *Nature* **396**, 239–242 (1998).
27. Ogilvie, J. P., Kubarych, K. J., Alexandrou, A. and Joffre, M., "Fourier transform measurement of two-photon excitation spectra: applications to microscopy and optimal control," *Opt. Lett.* **30**, 911–913 (2005).
28. Meshulach, D. and Silberberg, Y., "Coherent quantum control of multiphoton transitions by shaped ultrashort optical pulses," *Phys. Rev. A.* **60**, 1287–1292 (1999).
29. Walowicz, K. A., Pastirk, I., Lozovoy, V. V. and Dantus, M., "Multiphoton intrapulse interference. 1. Control of multiphoton processes in condensed phases," *J. Phys. Chem. A* **106**, 9369–9373 (2002).
30. Pang, S., Yeh, A. T., Wang, C. and Meissner, K. E., "Beyond 1/Tp limit: two-photon excited fluorescence using pulses as short as sub-10-fs," (forthcoming) (2008).
31. S.-C., Su, Mendoza, E. A., Kwak, H.-I. and Bayless, K. J., "Molecular profile of endothelial invasion of three-dimensional collagen matrices: insights into angiogenic sprout induction in wound healing," *Am. J. Physiol. Cell Physiol.* (forthcoming) (2008).
32. Yeh, A. T., Kao, B. S., Jung, W. G., Chen, Z. P., Nelson, J. S. and Tromberg, B. J., "Imaging wound healing using optical coherence tomography and multiphoton microscopy in an *in vitro* skin-equivalent tissue model," *J. Biomed. Opt.* **9**, 248–253 (2004).
33. Lansford, R., Bearman, G. and Fraser, S. E., "Resolution of multiple green fluorescent protein color variants and dyes using two-photon microscopy and imaging spectroscopy," *J. Biomed. Opt.* **6**, 311–318 (2001).
34. Dickinson, M. E., Simbuerger, E., Zimmerman, B., Waters, C. W. and Fraser, S. E., "Multiphoton excitation spectra in biological samples," *J. Biomed. Opt.* **8**, 329–338 (2003).
35. Buehler, C., Kim, K. H., Greuter, U., Schlumpf, N. and So, P. T. C., "Single-photon counting multicolor

multiphoton fluorescence microscope," *J. Fluoresc.* **15**, 41–51 (2005).
36. Palero, J. A., de Bruijn, H. S., van der Ploeg-van den Heuvel, A., Sterenborg, H. J. C. M. and Gerritsen, H. C., "*In vivo* non-linear spectral imaging in mouse skin," *Opt. Express* **14**, 4395–4402 (2006).
37. Ogilvie, J. P., Debarre, D., Solinas, X., Martin, J.-L., Beaurepaire, E. and Joffre, M., "Use of coherent control for selective two-photon fluorescence microscopy in live organisms," *Opt. Express* **14**, 759–766 (2006).
38. Radosevich, A. J., Bouchard, M. B., Burgess, S. A., Chen, B. R. and Hillman, E. M. C., "Hyperspectral *in vivo* two-photon microscopy of intrinsic contrast," *Opt. Lett.* **33**, 2164–2166 (2008).
39. Livet, J., Weissman, T. A., Kang, H., Draft, R. W., Lu, J., Bennis, R. A., Sanes, J. R. and Lichtman, J. W., "Transgenic strategies for combinatorial expression of fluorescent proteins in the nervous system," *Nature* **450**, 56–61 (2007).